Manufacturing of self-passivating tungsten based alloys by different powder metallurgical routes

A Calvo , N Ordás , I Iturriza , J Y Pastor , E Tejado , T Palacios and C García-Rosales

Abstract

Self-passivating tungsten based alloys will provide a major safety advantage compared to pure tungsten when used as first wall armor of future fusion reactors, due to the formation of a protective oxide layer which prevents the formation of volatile and radioactive WO_3 in case of a loss of coolant accident with simultaneous air ingress. Bulk WCr10Ti2 alloys were manufactured by two different powder metallurgical routes: (1) mechanical alloying (MA) followed by hot isostatic pressing (HIP) of metallic capsules, and (2) MA, compaction, pressureless sintering in H_2 and subsequent HIPing without encapsulation. Both routes resulted in fully dense materials with homogeneous microstructure and grain sizes of 300 nm and 1 μm, respectively. The content of impurities remained unchanged after HIP, but it increased after sintering due to binder residue. It was not possible to produce large samples by route (2) due to difficulties in the uniaxial compaction stage. Flexural strength and fracture toughness measured on samples produced by route (1) revealed a ductile-to-brittle-transition temperature (DBTT) of about 950 °C. The strength increased from room temperature to 800 °C, decreasing significantly in the plastic region. An increase of fracture toughness is observed around the DBTT.

Keywords: self-passivating tungsten alloys, plasma-facing material, mechanical alloying, HIP

Introduction

Tungsten is the main candidate plasma facing material for the first wall armor of future fusion reactors such as DEMO [1]. However, the use of pure W involves a potential safety risk in case of a loss-of-coolant accident, after which temperatures around 1000 °C are expected in the in-vessel components within several days because of the decay heat [2]. In such a situation, additional air ingress into the reactor vessel would lead to full armor oxidation and to the release of highly activated and volatile tungsten oxides [3]. The use of self-passivating tungsten alloys can be a feasible alternative to avoid this important safety issue: the alloying elements would form a stable oxide scale at high temperatures upon accidental air ingress, protecting the underlying W alloy from fast oxidation and sublimation of WO_3.

In previous work [4, 5] W–Cr–Si and W–Cr–Ti alloys were manufactured by mechanical alloying (MA) and densification of glass encapsulated powder by hot isostatic pressing (HIP). The addition of Cr and Si or Ti as alloying elements resulted in a reduction of the oxidation rate by several orders of magnitude at temperatures up to 1000 °C compared to pure tungsten [4, 6–8], due to the growth of a protective oxide layer. However, glass encapsulation is not suitable for manufacturing large samples due to their large weight, increasing the probability to leave out the capsule during HIPing. Thus, in the present work two different powder metallurgical (PM) routes are proposed as scalable methods to produce self-

Table 1. Relative density, microhardness and impurities content of WCr10Ti2 samples produced by the two PM routes.

	Relative density (%)	Microhardness ($HV_{0.5}$)	Impurities (wt%)		
			O	N	C
MA	—	—	0.11 ± 0.01	0.011 ± 0.001	0.016 ± 0.003
HIP	100	1015 ± 5	0.11 ± 0.01	0.010 ± 0.001	0.017 ± 0.002
Sintering	93	—	0.25 ± 0.06	0.012 ± 0.002	0.06 ± 0.01
Sinter. + HIP	100	865 ± 5	0.25 ± 0.05	0.011 ± 0.001	0.06 ± 0.01

passivating tungsten alloys. Route 1 consists of MA followed by HIP of metallic capsules containing the alloyed powder, whereas route 2 consists of MA, compaction, pressureless sintering in H_2 and subsequent HIPing without encapsulation. In this case, the goal is to produce a sintered material whose porosity is below 8% and closed, so that it can be completely removed by HIP. A similar route is used in industrial processes, where tungsten powder is sintered at high temperatures for long times to achieve porosities below 12% which can be eliminated by subsequent working, which also contribute to increase ductility and reduce the DBTT [9]. Si tends to form brittle intermetallics with detrimental effect on the workability. For this reason, efforts have been concentrated on Si-free alloys [5, 8]. In this work, alloys of composition WCr10Ti2 (in wt%) are manufactured by the two mentioned routes. A slightly lower Cr concentration with respect to previous work is employed since a minimum of the oxidation rate is achieved in binary W–Cr alloys for $\geqslant$10 wt% Cr [10]. Microstructure and impurity content of samples obtained by the two routes are compared, and mechanical properties of samples manufactured by the route 1 are shown.

Experimental details

Elemental powders of pure W (99.97%, 4.45 μm), Cr (99.95%, 74 μm) and Ti (99.5%, 40 μm) were used to produce samples of composition WCr10Ti2 in wt% (WCr27Ti6 in at%). The starting powders were mechanically alloyed under Ar in a planetary ball mill Retsch PM400 using WC grinding jars and balls. The MA parameters were those found as optimum for W–Cr–Ti systems in previous works [4, 5]. Samples of different geometries were produced with the milled powders by the two mentioned routes. In route1 metallic capsules of Ø 15 and 40 mm height filled with the alloyed powder were degassed at high vacuum, sealed and HIPed at 1300 °C for 1 h at 150 MPa. In route 2 the alloyed powder was uniaxially compacted at various pressures to cylinders of Ø 16 and 20 mm, and ~4 mm height, degassed at high vacuum and sintered at 1600 °C during 2 h under pure H_2. Organic binders were used for compaction. After sintering, the samples were HIPed without encapsulation at 1300 °C for 1 h at 150 MPa.

The particle size distribution of the milled powders was measured by laser diffraction. The oxygen and nitrogen contents of powders after MA and bulk materials obtained by both routes were determined using the inert gas fusion method (ASTM E1569, measured with a LECO TC-400), and the carbon content by the combustion method (ASTM E1019, measured with a LECO CS-200). Powders and bulk samples were characterized by field emission gun SEM (FEG-SEM), energy dispersive x-ray spectroscopy (EDX) and x-ray diffraction (XRD). The open porosity after sintering was measured by He pycnometry, and the relative density of all samples was determined from the geometrical and theoretical densities. The average grain size of the materials was determined by quantitative metallography.

Vickers microhardness of HIPed materials was measured applying a load of 0.5 kg for 5 s. The elastic modulus was measured up to 1000 °C by the Impulse Excitation Technique (IET) on samples of dimensions $5 \times 2 \times 30\,mm^3$. Three-point bending (TPB) tests were performed on smooth and single edge laser-notched beams [11] (nominal dimensions $2.5 \times 2.5 \times 30\ mm^3$) over the temperature range 20 °C to 1100 °C under high vacuum. All tests were performed in displacement control at a fixed loading rate of 100 μm/min with 25 mm span width. Flexural strength was computed by Euler–Bernoulli equations for slender beams up to failure. However, when yield stress was exceeded, 0.2% strength offset was reported. To calculate fracture toughness (K_{IC}), the maximum load and the initial notch length for each test, measured previously via FEG-SEM, were computed in the formula proposed by Guinea *et al* [12].

Results and discussion

Mechanically alloyed powders of composition WCr10Ti2 in wt% (WCr27Ti6 in at%) were used to produce dense materials by the two PM routes. The particle size of the powders after MA exhibits a bimodel distribution with peaks at 4.5 and 12 μm. Their O, C and N contents are shown in table 1.

Route 1: MA + HIP with can encapsulation

The mechanically alloyed powders were can encapsulated and HIPed at 1300 °C for 1 h achieving relative densities above 99%, i.e. the samples can be considered fully dense within the experimental error. The O, C and N contents of the as-HIPed materials (table 1) indicate that there is no uptake of contaminants during encapsulation and HIPing. The amounts of O and C after HIP are comparable to those reported in previous works using glass encapsulation [4, 5].

The microstructure of WCr10Ti2 samples is shown in figures 1(a), (b). A very fine and homogenous microstructure

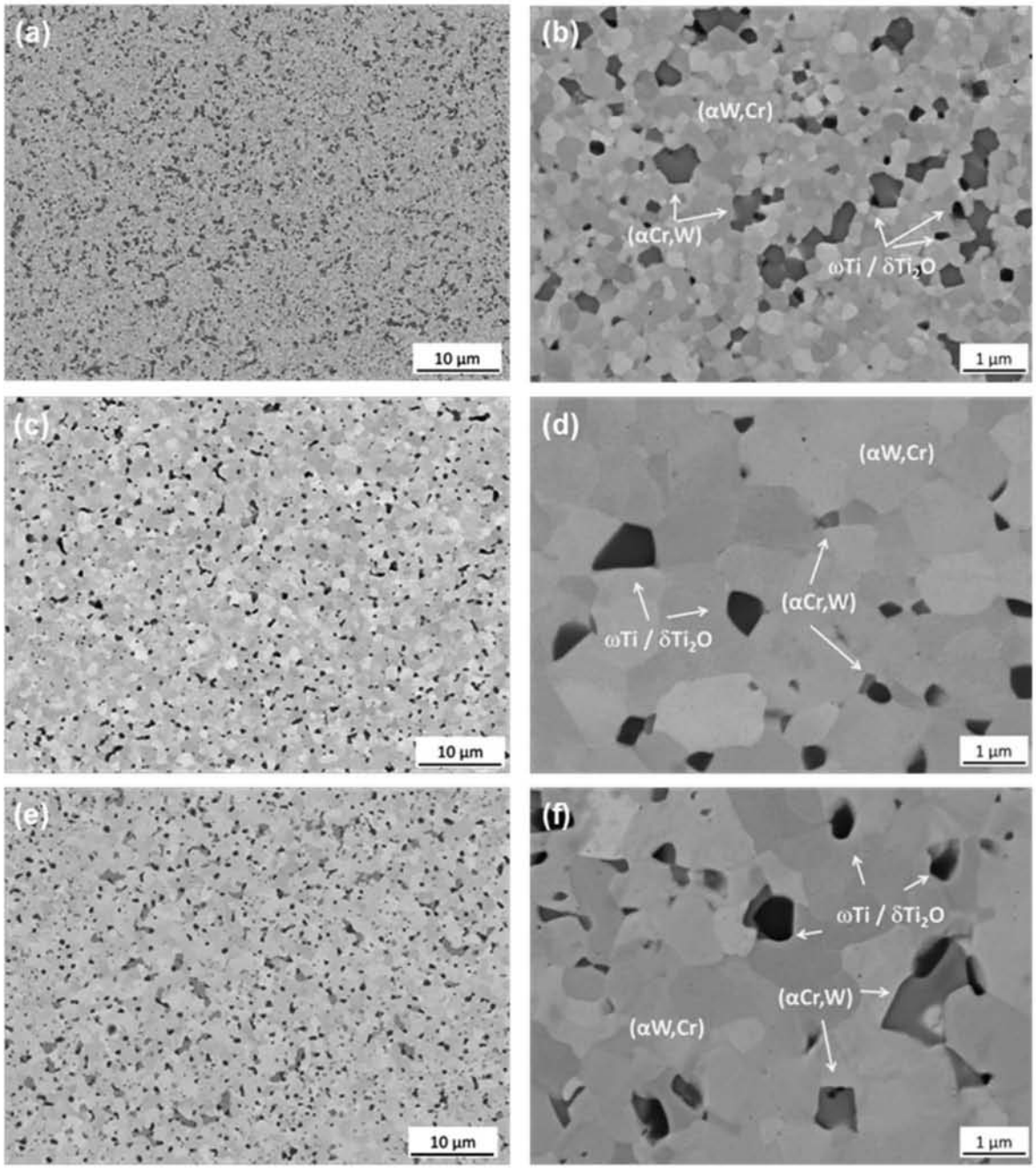

Figure 1. FEG-SEM images of WCr10Ti2 alloy after HIP at 1300 °C (a)–(b), after sintering at 1600 °C (c)–(d) and after sintering at 1600 °C + HIP at 1300 °C (e)–(f).

with average grain size 210 ± 20 nm can be appreciated. As already found in previous work for a slightly different composition [5], the material is composed of three phases, identified by EDX as a W-rich phase with Cr in solution (bright gray majority phase in figures 1(a) and (b)), a Cr-rich phase with W in solution (dark gray discontinuous phase) and a minority Ti-rich phase (black), which is mainly found in connection with the Cr-rich phase. EDX analysis of this Ti-rich phase evidences the presence of oxygen.

In figure 2 the XRD spectra of the initial and mechanically alloyed powders and of the bulk materials produced with the two routes are compared. After MA, a single bcc phase is observed with broad peaks shifted to higher 2θ values compared to the pure W phase indicating the dissolution of Cr in the W lattice; Ti is most probably also dissolved in W, but the 2θ shift produced by the small amount of Ti present in the mix would not be appreciated due to the similar lattice parameters of W and the high temperature bcc Ti phase [13]. The amount of Cr dissolved in the W lattice can be estimated from the shift of the XRD peaks using the Vegard's law [14], and is about 20 at%, i.e. after MA a supersaturated (αW,Cr) phase is formed. The missing Cr amount of about 9 at% is

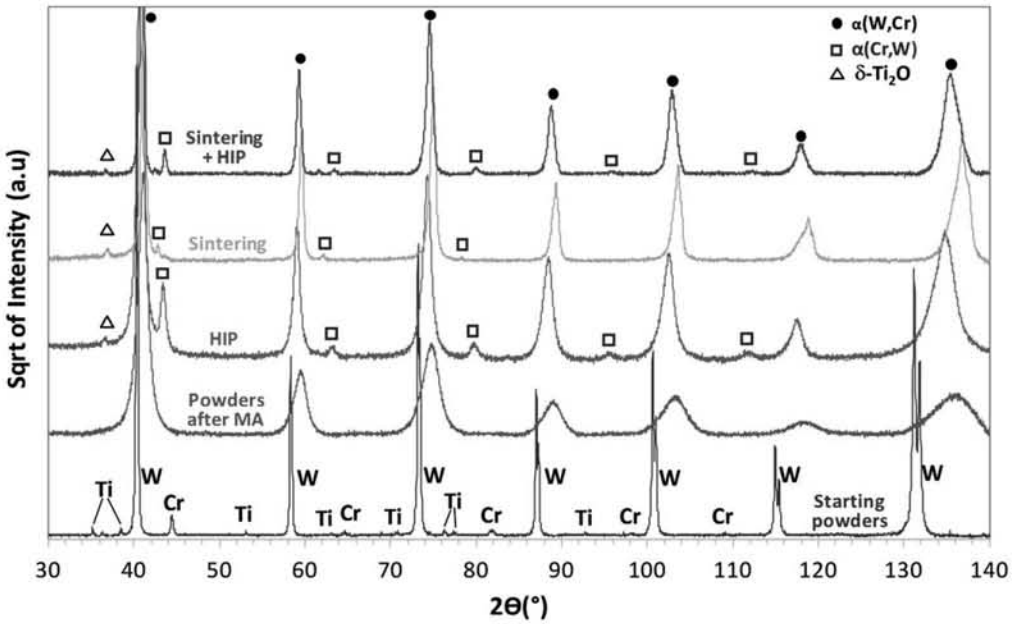

Figure 2. XRD spectra of WCr10Ti2 samples after HIP at 1300 °C, sintering at 1600 °C and sintering at 1600 °C + HIP at 1300 °C.

probably found in the initial pure Cr phase, which may have also W in solution and whose peaks cannot be appreciated due to the broadening induced by the MA process.

After HIPing at 1300 °C the broad (αW,Cr) peaks present after MA are shifted to lower 2θ values indicating a decrease in the Cr content, which is now of the order of 15 at%, and a (αCr,W) phase containing about 22 at% W dissolved in bcc Cr emerges. The peaks after HIP are still quite broad suggesting that a homogeneous phase composition has not yet been achieved. Nevertheless, the compositions of the (αW,Cr) and (αCr,W) phases are close to those expected at equilibrium at 1300 °C as determined with the Thermo-Calc software [15] using the SSOL4 solutions database. The identification of the Ti-rich phase by XRD is not evident since only one peak at $2\theta \approx 36°$ is fully resolved. In previous work [5] this phase had been identified as ω-Ti, a metastable phase formed both in the Ti–W and Ti–Cr system during quenching from the bcc high temperature phase [16]. Nevertheless, the equiaxed form and size of the Ti-rich grains indicate that this phase nucleates at high temperature at the same time as the (αW,Cr) and (αCr,W) phases. The ω-Ti phase is also a high-pressure phase formed from the parent bcc Ti phase [16]. According to EDX the whole oxygen content of the alloy seems to be associated to this phase. From all possible Ti-oxides, δ-Ti_2O [17] is the one better matching the XRD peaks. In this oxide the Ti subarray is identical to the high-pressure ω-Ti phase [18], and according to [19] the oxygen provides the pressure medium that stabilizes this phase. Taking into account the Ti and O contents in the alloy of 2 and 0.11 wt% respectively (6 and 1 at% respectively), it becomes clear that only 2 at.% Ti can form δ-Ti_2O and the remaining 4 at% are possibly in form of ω-Ti or in solution with W and Cr as expected from the phase diagram.

The room temperature (RT) Vickers microhardness of HIPed WCr10Ti2 samples (table 1) is significantly higher than the one of pure recrystallized tungsten (∼380 HV30) [9]. However, the hardness of polycrystalline tungsten increases appreciably with decreasing grain size following a Hall–Petch relationship [9]. Taking into account the average grain size of the WCr10Ti2 alloy of 209 nm, the measured hardness would be in line with that of pure tungsten for similar grain size [9]. Nevertheless, both solution and precipitation hardening are also expected to contribute to an alloy hardness increase, indicating that the WCr10Ti2 alloy may exhibit different Hall-Petch constants leading to lower grain-boundary strengthening compared to pure tungsten.

Samples of WCr10Ti2 alloy produced by route 1 were manufactured to explore its mechanical response by non-standard TPB tests and its elastic modulus by IET. It should be noted that, while normally the MA process results in homogeneous powders with low amounts of heterogeneities (figure 1(a)), the powder batch produced for these samples exhibited abnormally large amounts of heterogeneities, which were detected once the samples were cut out of the HIPed cylinder. These heterogeneities may act as crack initiation defects and so the resulting strength values will most probably be underestimated.

The run of the elastic modulus curve as a function of temperature is very similar to that of polycrystalline tungsten [9] while the values of the WCr10Ti2 alloy are ∼20% lower in the measured temperature range of RT to 1000 °C.

The flexural strength and fracture toughness of the as-HIPed material are presented in figure 3. The smooth bars tested under TPB presented linear load–displacement curves up to 900 °C, above which brittle-to-ductile transition takes place. As observed in figure 3 (left), WCr10Ti2 exhibits a clear increase in strength between 20 and 800 °C, reaching a

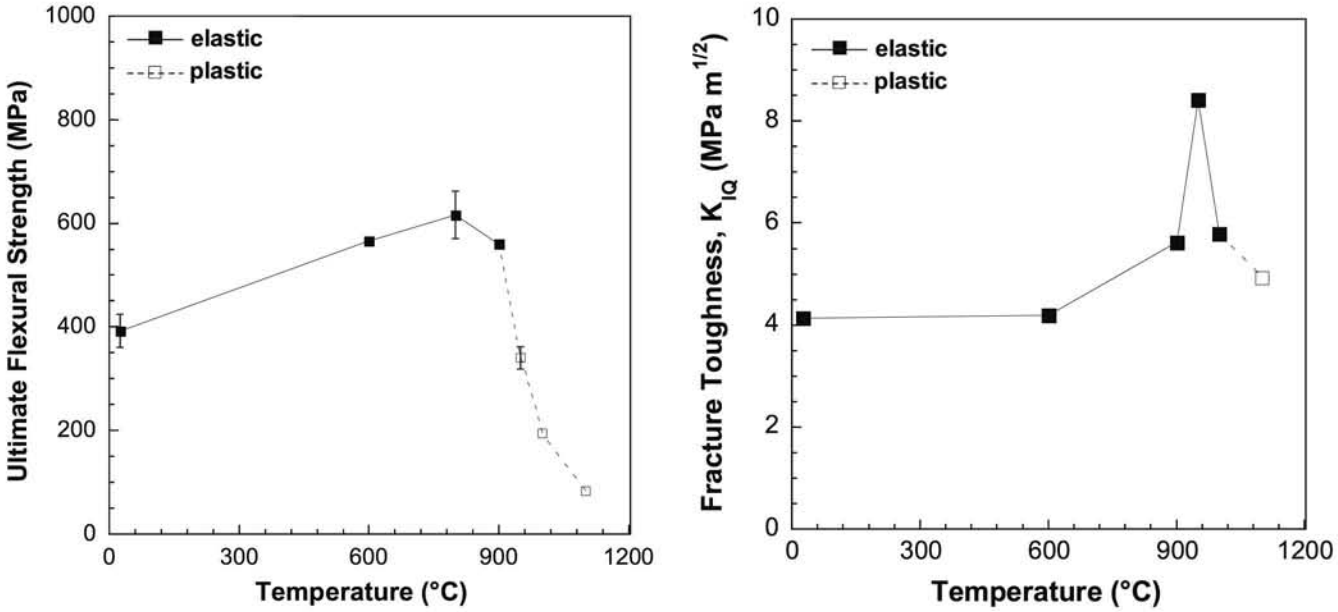

Figure 3. Average flexure strength (left) and average fracture toughness (right) versus test temperature for WCr10Ti02 after HIP at 1300 °C. In the left figure open symbols represent the yield strength at 0.2%. In the right figure continuous lines and full symbols represent the linear elastic behavior (fracture toughness) whereas open symbols denote the plastic behavior (apparent fracture toughness).

maximum strength of 616 MPa and then decreasing in the plastic region. In figure 3 (right) the fracture toughness as a function of temperature is plotted. In most cases, the load–displacement curves were linear up to fracture, and the fracture toughness was computed from the maximum load and the initial notch length in each test using the appropriate expression for the stress intensity factor [12]. The results displayed show that the material appears to attain the highest values at 950 °C, i.e. around the DBTT, decreasing beyond this temperature. Its behavior with temperature is consistent with that found for the flexural strength.

Route 2: MA + Compaction + Pressureless Sintering in H2 + HIP without encapsulation

After pressureless sintering at 1600 °C the samples of Ø16 mm exhibited 93% relative density whereas those of Ø20 mm did not reach 90% due to the presence of cracks by end-capping. The compaction stage is not easy because of the high hardness and difficult deformation of the alloyed powder. For this reason, it was necessary to add a binder. Since samples with 93% density exhibited entirely closed porosity, they were HIPed without encapsulation at 1300 °C and 150 MPa for 1 h, achieving 100% density. Nevertheless, the O and C contents of these samples increased by a factor of about 2 and 4, respectively (table 1), due to the binder residue. Again, no uptake of contaminants was detected after HIP.

After sintering at 1600 °C the microstructure was fine and homogeneous with an average grain size of 980 ± 30 nm (figures 1(c) and (d)). The main phase corresponds to (αW, Cr) with small amounts of (αCr,W) and Ti-rich phases. The approximate composition of the two bcc phases can be deduced from the shift of the corresponding XRD peaks (figure 2). The (αW,Cr) phase has a Cr content of about 23 at% while the (αCr,W) phase, with a hardly visible peak, has a W content of about 38 at%. According to the phase diagram, for the present alloy composition at 1600 °C only one single bcc phase should be present. The composition of the (αW,Cr) phase corresponds in the W–Cr phase diagram to a temperature of the order of 1450 °C. This fact together with the broadness and asymmetric shape of these peaks in the corresponding XRD spectrum of figure 2 indicate that longer sintering times would be required to achieve the composition of equilibrium.

After a subsequent HIP cycle at 1300 °C the microstructure (figures 1(e)–(f)) is similar to the one after sintering with the difference of a larger presence of the (αCr,W) phase, as expected according to the phase diagram. The compositions of the (αW,Cr) and (αCr,W) phases with about 17 at% Cr and 21 at% W, respectively, correspond to a temperature in the W–Cr phase diagram of about 1350 °C, indicating that again longer times are required for achieving the composition of equilibrium.

The Vickers microhardness of the WCr10Ti2 alloy after sintering + HIP (table 1) is lower than the one of the material produced by route 1 due to the grain growth during sintering at 1600 °C. Using the Hall-Petch relationship of polycrystalline tungsten [9] to determine its hardness for the same average grain size as in this case (984 nm), a value about 20% lower is obtained, indicating that in the WCr10Ti2 alloy produced by route 2 precipitation hardening may stronger contribute to grain-boundary strengthening compared to the alloy produced by route 1, probably due to the higher O and C contents.

Because of the difficulties in manufacturing large samples, no mechanical properties have been measured on samples produced by this route. Compaction by cold isostatic pressing in the future would be a feasible way to overcome

these problems, avoiding also the use of binder and thus the introduction of undesired contamination.

Conclusions

Self-passivating bulk WCr10Ti2 alloys were manufactured by two different powder metallurgical routes. Route 1 consists of MA followed by HIP of metallic capsules whereas route 2 consists of MA, compaction, pressureless sintering in H_2 and subsequent HIPing without encapsulation. Both routes result in fully dense materials with a very fine and homogeneous microstructure consisting of two main phases, (αW,Cr) and (αCr, W), and a minority phase corresponding probably to ω-Ti/δ-Ti_2O. Grain sizes about 300 nm and 1 μm were found for the materials produced by routes 1 and 2, respectively. The content of impurities after MA was reasonably low and remained unchanged after HIP, but it increased after sintering due to the binder residue. It was not possible to produce large samples by route 2 due to difficulties in the uniaxial compaction stage.

Flexural strength and fracture toughness was measured on samples produced by route 1. The DBTT is of the order of 950 °C. The strength increases from room temperature to 800 °C and decreases significantly in the plastic region. An increase of fracture toughness is observed around the DBTT.

Acknowledgments

This work has been carried out within the framework of the EUROfusion Consortium and has received funding from the Euratom research and training program 2014-2018 under grant agreement No 633053, by the Spanish Ministry of Economy and Competitiveness (ENE2012-30753 and MAT2012-38541-C02-02) and by Comunidad de Madrid (research project S2013/MIT-2862-MULTIMAT-CHALLENGE). The views and opinions expressed herein do not necessarily reflect those of the European Commission.

References

Stork D *et al* 2014 *Fusion Eng. Des.* **89** 1586
Maisonnier D *et al* 2005 A conceptual study of commercial fusion power plants *Final Report* EFDA-RP-RE-5.0
Taylor N P and Pampin R 2006 *Fusion Eng. Des.* **81** 1333
López-Ruiz P, Ordás N, Lindig S, Koch F, Iturriza I and García-Rosales C 2011 *Phys. Scr.* **T145** 014018
López-Ruiz P *et al* 2013 *J. Nucl. Mater.* **442** 219
García-Rosales C, López-Ruiz P, Alvarez-Martín S, Calvo A, Ordás N, Koch F and Brinkmann J 2014 *Fusion Eng. Des.* **89** 1611
Koch F, Köppl S and Bolt H 2009 *J. Nucl. Mater.* **386–8** 572
Koch F, Brinkmann J, Lindig S, Mishra T P and Ch L 2011 *Phys. Scr.* **T145** 014019
Lassner E and Schubert W-D 1999 *Tungsten, Properties, Chemistry, Technology of the Element, Alloys and Chemical Compounds* (Vienna: Kluwer)
Brinkmann J 2015 (Max-Planck-Institute for Plasma Physics) private communication
Palacios T and Pastor J Y 2015 *Int. J. Refract. Met. Hard Mater.* **52** 44
Guinea G V, Pastor J Y, Planas J and Elices M 1998 *Int. J. Fract.* **89** 103
Nagender Naidu S V and Rama Rao P 1991 *Phase Diagrams of Binary Tungsten Alloys* (Calcutta: Indian Institute of Metals)
Vegard L 1921 *Z. Phys.* **5** 17
Andersson J O, Helander T, Höglund L, Shi P F and Sundman B 2002 Thermo-Calc and DICTRA, computational tools for materials science *Calphad* **26** 273–312
Sikka S K, Vohra Y K and Chidambaram R 1982 *Prog. Mater. Sci.* **27** 245
Andersson S 1959 *Acta Chem. Scand.* **13** 415
Akahama Y, Kawamura H and Le Bihan T 2001 *Phys. Rev. Lett.* **87** 275503
Vegas A *et al* 2004 *Solid State Sci.* **6** 809